Systematic analysis and modification of embedded-atom potentials: Case study of copper

Jari Jalkanen and Martin H. Müser ‡

Forschungszentrum Jülich GmbH, Institute for Advanced Simulation (IAS), Jülich Supercomputing Centre (JSC), Wilhelm-Johnen-Straße, 52425 Jülich, DE

July 2014

Abstract. In this study, we analyze the performance of different embedded-atom models (EAM) by fitting their free parameters to ab-initio results for copper. Our emphasis lies on testing the transferability of the potentials between systems which vary in their spatial dimension and geometry. The model structures encompass zero-dimensional clusters, one-dimensional chains, two-dimensional tilings, and three-dimensional bulk systems. To avoid having to mimic charge transfer, which is outside the scope of conventional EAM potentials, we focus on structures, in which all atoms are symmetrically equivalent. We find that the simple, four-parameter Gupta EAM potential is overall satisfactory. Adding complexity to it decreases the errors on our set of structures only by marginal amounts, unless EAM is modified to depend also on density gradients, higher-order derivatives, or related terms. All tested conventional EAM potentials reveal similar problems: the binding energy of closed-packed systems is overestimated in comparison to open or planar geometries, and structures with small coordination tend to be too rigid. These deficiencies can be fixed in terms of a systematically modified embedded-atom method (SMEAM), which reproduces DFT results on bond lengths, binding energies, and stiffnesses or bulk moduli by typically $O(1\%)$, $O(5\%)$, and $O(15\%)$ accuracy, respectively. Yet, SMEAM does not overcome the difficulty to reproduce the elastic tensor elements of a hypothetical diamond lattice.

Submitted to: *Modelling Simul. Mater. Sci. Eng.*

1. Introduction

The embedded-atom method (EAM) has proven invaluable for the simulation of bulk metals. [1, 2, 3, 4, 5] It dramatically alleviates several shortcomings of pair potentials without a significant overhead in CPU time. When properly parametrised, EAM can reproduce the way in which real metals violate the Cauchy relation, while pair potentials automatically obey it. [6] In pair-potential crystals, the spacing between layers increases towards the surface, whereas in real and EAM metals it decreases. [7, 8] Pair potentials predict the binding energy per atom E_0 to scale approximately linearly with

‡ Corresponding author, e-mail:m.mueser@fz-juelich.de

the coordination number Z, while $E_0 \propto \sqrt{Z}$ is a more reasonable approximation for real metals, [9] which can be easily reproduced with EAM. [10] Likewise, the energy of a point vacancy defect, E_v, is roughly proportional to the number of nearest neighbors in a pair-potential description. As a consequence, for pair potentials $E_\mathrm{v} \approx E_0/2$, while real and EAM point defects cost substantially less energy. [11, 12] Similar trends hold for other defect energies, such as surface energies. Since defect energetics determine the failure mechanisms of a material, [13, 14] EAM-based potentials possess a better ability than pair potentials to describe realistically not only the elastic tensor and the structural relaxation of surfaces but also the plastic response of metals.

Quite a few different embedded-atom-type methods exist. Different variants may even claim their own names, such as the glue-, [15, 16] the Finnis-Sinclair- [17] or the effective-medium potential. [18, 19] Yet they all share one fundamental assumption from quasi-atom theory: [20] embedding an atom i at $\mathbf{r}_i$ into the environment of other atoms leads to an embedding energy $F(\rho_i)$ that depends in leading order on the (estimated) electronic density that exists at $\mathbf{r}_i$ before the atom is embedded. In addition, a pairwise repulsion between atoms is usually assumed. As such, the total energy of a configuration $\{\mathbf{r}\}$ can be cast as

$$V_\mathrm{tot}(\{\mathbf{r}\}) = \sum_{i,i<j} V_\mathrm{R}(r_{ij}) + \sum_i F(\rho_i) \tag{1}$$

for the simplest EAM variants, where in most cases the charge density results from a linear superposition of atom-centered charge densities, i.e.,

$$\rho_i = \sum_{j\neq i} f_j(r_{ij}). \tag{2}$$

Density gradients or higher-order derivatives are assumed of negligible importance. For alloys, which shall not be considered here, $V_\mathrm{R}(r_{ij})$, $F(\rho_i)$, and $f_j(r_{ij})$ need to be indexed by the atom type(s) as well. EAM potentials can differ in the choice of the functions $V_\mathrm{R}(r)$, $F(\rho)$, and $f(r)$ ranging from simple analytical expressions to elaborate, implicitly defined functions. However, it is not clear to what degree algebraically complex EAM potentials outperform simple variants, and if so, what the relevant "ingredients" are. In this paper, we want to address this question by investigating the performance of EAM potentials on a broad set of copper structures. The study includes potentials, in which different aspects of existing potentials were combined and more importantly extended according to ideas motivated from quasi-atom theory.

Since most EAM-based simulations are supposed to address bulk mechanical properties, free parameters are typically fitted to a set of structures biasing the potential towards the particular research interests of the force-field developer, which can range from grain boundaries and bulk plasticity to modeling indentation experiments or properties of the liquid phase. [21, 22, 23, 24] Important quantities to match in such contexts are point-defect and surface energies. Using this fitting strategy, one can reproduce some of the desired quantities quite accurately, but potentially only "by accident:" metal surfaces tend to have a surface dipole, which means that the metal

has decreased its energy through the internal redistribution of charge, although it costs energy to create the related electrostatic fields. Conventional EAM cannot reflect this situation, because atoms can neither polarize nor exchange charge. Even the charge-transfer EAM potential by Streitz and Mintmire cannot account for the effect, [25] as long as the electronegativity of atoms is not made environment dependent. [26] For an application-driven parameterization, it is certainly legitimate, if not desirable, to "fudge" effects due to internal charge redistribution, or also due to Jahn–Teller and Peierls deformations, into the EAM parametrisation. If, however, we want to apply the potential to heterogeneous environments, this course of action might impede its reliability or transferability.

To test and, ultimately, to design EAM potentials in a systematic fashion, we see it as beneficial to first restrict the analysis to situations in which charge transfer is excluded. This way, parameters can be determined in a robust fashion and do not have to change significantly under circumstances whose proper description may necessitate additional terms. In the current study, we therefore concentrate on structures, in which each atom of a given configuration is embedded into an exactly identical environment and defer the inclusion of charge-transfer and a systematic analysis of Jahn–Teller or Peierls deformation to future work. Thus, in contrast to existing tests of EAM potentials, [4, 27] the primary goal of our work is to identify the EAM formulation with the greatest prospect to be used as a basis for (systematic) generalizations or transferability rather than to identify EAM parameters that are most accurate for a particular application.

Our material of choice is copper, as it appears to be the element that has been most modeled with EAM. Transferability of the potentials is tested with regard to bonding environments ranging from $Z = 1$ to $Z = 12$, different bond angles, and dimensionalities of the structures. Transferability with respect to alloying is not considered.

The remainder of this work is organised as follows: Methods are described in section 2. This includes the description of different EAM approaches and a systematic formulation or extension of the modified embedded-atom method. In section 2, we also discuss the investigated reference structures, define and motivate observables as well as the χ^2 goodness function, and describe the DFT methods used to produce the reference data. Section 3 contains the results of our fits. First, this is done such that we take the simple, four-parameter Gupta EAM as a reference, [28] and alter one aspect at the time, e.g., by replacing the simple embedding function or the charge-density function with more elaborate expressions. Later, we also test select, complete potentials, in which all terms have their original complexity. Conclusions are drawn in the final section 4.

2. Methods

2.1. Popular Embedding-Atom Methods

In this section we briefly sketch the most important equations of the EAM methods tested in this study. The fundamental ideas underneath EAM-based potentials have

been summarised numerous times in the literature, [3, 20, 23, 17, 29, 30] to which we refer the reader for detailed accounts. Here, it shall suffice to mention that the central aspect of embedded-atom methods can be motivated from the bottom up via the classical theorem by Hohenberg and Kohn. It states that for a given external electric field, produced, e.g., by nuclear positions, the ground state energy of an associated electronic system is a unique functional of the electronic density. In a loose sense, one could interpret the term $F(\rho)$ in equation (1) to realize a coarse-grained version of that theorem for the bonding electrons, while the additional repulsive term takes into account the unscreened direct repulsion between the nuclei and the Pauli repulsion between the core electrons in a more phenomenological fashion. Deeper connections of the embedding energy terms and the most common functionals of DFT have been made, [31] though it is not always clear if the gained insights help in practice.

In the remaining part of this model section, we review some of the most popular choices for the various terms arising in different EAM variants and introduce the acronym for each EAM component. Complete potentials then arise as combinations of these terms. They are defined in the results section. Here, it is sufficient to state that we choose the functional form proposed by Gupta, [28] as a reference, and then only change either repulsion, charge density or the embedding function, one at a time. This choice is motivated partly because the Gupta potential produces good results. More importantly, its simplicity allows us to rationalize properties generic for all EAM potentials with back-of-the-envelope calculations, which we also present in this section. Finally, we construct systematically corrections due to (estimated) density gradients and terms related to higher-order derivatives.

2.1.1. Charge Density. The function $f_j(r_{ij})$ in equation (2) is supposed to represent the electronic charge density at the position $\mathbf{r}_i$ that is due to the presence of all other atoms j located at $\mathbf{r}_j$ before atom i is embedded. When treating alloys, each function f_j should scale as the inverse atomic volume in order to represent a charge density. This prefactor can be absorbed into the embedding function for a mono-atomic system.

As a zeroeth-order approximation, one may choose $f_j(r)$ to be proportional to the charge density of the free atom. In this spirit, Daw and Baskes [32] proposed to use the double-gamma function originally calculated by Clementi and Roetti: [33]

$$f_j(r) = \sum_{n=3d,4s} \frac{N_n}{4\pi r} \rho_j^{(n)}(r) \qquad \text{(C-DG)} \tag{3}$$

$$\rho_j^{(n)}(r) = \left| \sum_{k=1\ldots l_n} c_{nk} \frac{(2r\gamma_{nk})^{\lfloor k/2 \rfloor + 1/2}}{\sqrt{(2\lfloor k/2 \rfloor)!}} e^{-\gamma_{nk} r} \right|^2 . \tag{4}$$

For copper, $N_{3d} = 10$, $N_{4s} = 1$, $l_{3d} = 8$, and $l_{4s} = 2$. The symbol $\lfloor ... \rfloor$ represents the floor function. For the coefficients c_{nk} and γ_{nk}, we refer the reader to reference. [33] Note that the index n in equation (3) does not enumerate atoms that a central atom is interacting with but the valence shells of copper or a related transition metal. Since the coefficients of the double-gamma functions follow from a free-atom Hartree-Fock calculation, there

are no further tunable parameters. In the following, the acronym C-DG represents a model in which the charge density is represented by a double-gamma function in the just-mentioned fashion.

In most applications of practical interest, nearest neighbors are located at distances where the contribution of $4s$ electrons is largest. Consequently the shape of the double-gamma function is relatively tame between typical nearest to next-nearest neighbor distances. This is one reason why several authors replaced the original form with algebraically simpler functions. For our study, we selected the exponential (C-Exp), equation (5), the Gaussian (C-Gauss), equation (6), and the inverse monomial (C-IM), equation (7) charge densities introduced by Finnis and Sinclair, [34] and later studied by Sutton and Chen, [35] equation (7):

$$f(r) = \exp(-r/\sigma_{\mathrm{Q}}) \qquad \text{(C-Exp)} \tag{5}$$

$$f(r) = \exp\left\{-r^2/\left(2\sigma_{\mathrm{Q}}^2\right)\right\} \qquad \text{(C-Gauss)} \tag{6}$$

$$f(r) = r^{-\alpha} \qquad \text{(C-IM).} \tag{7}$$

Sometimes $f(r)$ is cut off at an appropriate cutoff radius R_{c}, which may involve smoothing $f(r)$ to cause it — and potentially also its first derivative — go to zero continuously.

We note in passing that the exponent α in the C-IM approach was set to $\alpha = 6$ by Finnis and Sinclair. [34] The value of the exponent is not associated with dispersive interactions but instead has its origin in s-d hopping integrals scaling as $1/R^6$. [36] When using α as adjustable fit parameter, it generally turns out to be close to six.

Rather than simplifying the C-DG ansatz, there were also attempts, e.g., by Baskes, [37, 38] in the modified embedded-atom method (MEAM), to add *more* complexity and realism. This led to expressions for an effective charge density involving products of one, two, or three components of the radius vector between the charge-density-donating atom and the central atom. Through such measures, $F(\rho)$ becomes sensitive to the way in which other charges are arranged around the central atom and not only to the number of neighbors at given distances.

In the following, C-MEAM refers to approaches in which a generalised density, $\rho_i^{(\mathrm{g})}$, as proposed in reference [38], is used as density in the embedding function, rather than the zero-order guess ρ_i from equation (2). We write the generalization as

$$\rho_i^{(\mathrm{g})} = \sqrt{\rho_i^2 + 4c_{\mathrm{G2}}\rho_{i\alpha}^2 + 4c_{\mathrm{H2}'}\rho_{i\alpha\beta}^2 + 4c_{\mathrm{T2}}\rho_{i\alpha\beta\gamma}^2} \tag{8}$$

where we have used the summation convention for Cartesian coordinates (Greek indices) — i.e., we sum over any index appearing twice, e.g., $\rho_{i\alpha}^2 \equiv \sum_\alpha \rho_{i\alpha}^2$ — and where

$$\rho_{i\alpha} = \sum_j (\mathbf{n}_{ij})_\alpha f_1(r_{ij}) \tag{9}$$

$$\rho_{i\alpha\beta} = \sum_j (\mathbf{n}_{ij})_\alpha (\mathbf{n}_{ij})_\beta f_2(r_{ij}) \tag{10}$$

$$\rho_{i\alpha\beta\gamma} = \sum_j (\mathbf{n}_{ij})_\alpha (\mathbf{n}_{ij})_\beta (\mathbf{n}_{ij})_\gamma f_3(r_{ij}), \tag{11}$$

with

$$f_n = e^{-r_{ij}/\sigma_{\mathrm{Q}n}} \tag{12}$$

and $\mathbf{n}_{ij}$ being a unit vector pointing from atom i to atom j. In equations (8)–(11), the summation over j is often constrained to all nearest-neighbor indices of the central atom i. Original numerical values for the parameters $c_{\mathrm{G}2}$, $c_{\mathrm{H}2'}$, $c_{\mathrm{T}2}$ and $\sigma_{\mathrm{Q}n}$ can be deduced from the literature. [38] We depart from the original MEAM notation to facilitate the connection to SMEAM.

2.1.2. Embedding Functions. As is the case for the charge density, many possibilities exist to design the embedding function $F(\rho)$. In an influential work, [32] Daw and Baskes proposed to choose $F(\rho)$ such that for a given pair repulsion, the experimental equation of state (EOS) of a reference structure, in which each atom is equivalent (e.g., fcc) is reproduced exactly. This can be achieved if the embedding function is defined implicitly via

$$F\{\rho_{\mathrm{fcc}}(a)\} = E_{\mathrm{fcc}}\{a(\rho_{\mathrm{fcc}})\} - \frac{1}{2}\sum_j V_{\mathrm{R}}\left\{g_j^{\mathrm{fcc}} a(\rho_{\mathrm{fcc}})\right\} \qquad \text{(E-EOS)} \tag{13}$$

Here, $a(\rho_{\mathrm{fcc}})$ denotes the nearest-neighbor spacing at which the charge density ρ on a given atom takes the value $\rho = \rho_{\mathrm{fcc}}$ for our fcc reference lattice. We compute it as the inverse function of $\rho_{\mathrm{fcc}}(a)$ through a golden section search. $E_{\mathrm{fcc}}\{a\}$ stands for the energy per atom, which is deduced from the EOS. The dimensionless number g_j states the distance between the central atom and atom j in units of the nearest-neighbor distance. This way of parameterizing the embedding function guarantees some "exact" results — in the sense of an exact reproduction of the input data — for all physical properties that follow from the fcc EOS. This includes the fcc cohesive energy, bulk modulus, and lattice constant at ambient pressure.

In practice, the EOS is often approximated with analytical expressions, in which case $F(\rho)$ can be written down explicitly. Some of these approximations are highly accurate under conditions of elevated pressure but unsuitable for the EAM calculations, because they produce an incorrect dissociation limit. In their original work, Daw and Baskes chose the Rose-Vinét equation, [39] which leads to the correct dissociation limit, i.e., $E(a \to \infty) = 0$ and thus $F(\rho \to 0) = 0$. As an alternative, we consider the Birch-Murnaghan EOS, [40] which only satisfies the dissociation limit if the pressure derivative of the bulk modulus at zero pressure, $B'(p=0)$, is set to $6 - 16E_0\sqrt{2}/9Ba_0^3$, where E_0, B and a_0 are the equilibrium cohesive energy, bulk modulus and bond length of the system under consideration. For an fcc Cu crystal, this relation results in $B'(p=0) \approx 5.4$, which happens to be close to the experimental value [41] of 5.59.

In later work, Baskes used an analytical form for the embedding function in the context of the MEAM approach:

$$F(\rho) = A\rho\ln(\rho/\rho_0) \qquad \text{(E-MEAM)}, \tag{14}$$

where A and ρ_0 are adjustable coefficients. The functional form of $F(\rho)$ was motivated from the logarithmic dependence of the bond length on coordination number, [37] though other embedding functions actually reproduce the correct trend, as demonstrated in section 2.3.

In reference to the valence bond theory by Friedel [42, 43], Gupta argued that the embedding energy should roughly scale with the square root of the coordination number. [28] This lead to the embedding function

$$F(\rho) = A\sqrt{\rho} \qquad \text{(E-Friedel)} \tag{15}$$

with just one adjustable (negative) coefficient A, which is also used by Sutton and Chen. [35] The $F \propto \sqrt{\rho}$ dependence can also be motivated from bond-order potentials, [44] in which case the density would be interpreted as the sum of the square over all bond integrals.

Another option is to simply use a truncated Taylor series expansion, see, e.g., Eq. (7.22) in [19] such as

$$F(\rho) = \sum_{n=1}^{n_{\max}} \frac{c_n}{n!}\rho^n \qquad \text{(E-Taylor)} \tag{16}$$

In this series, the leading-order linear term relates to a pair potential, as the linear term is pairwise additive, while the second-order derivative of the embedding function directly relates to the violation of the Cauchy relation. [32] Moreover, a polynomial expansion allows one to reproduce the trend that elements other than noble gases show a minimum in binding energy when being immersed into a constant electron density background. [45] Interestingly, the depth of these minima correlates well with the strength of bonds formed by the atom in question.

2.1.3. Repulsion. Repulsive interatomic interactions, other than those induced by like charges, are short ranged. One of the simplest functions mimicking repulsion, which was motivated in the early days of valence-bond theory from the Fermi exclusion principle, is the exponential

$$V_{\mathrm{R}}(r) = V_0 \exp(-r/\sigma_{\mathrm{R}}) \qquad \text{(R-Exp)}, \tag{17}$$

which we denote as R-Exp. In equation (17) and the following equations, V_0 and σ_{R} are (adjustable) numerical coefficients of unit energy and length, respectively.

Since the lengthscale, in which short-range repulsion matters for most applications, is limited to nearest-neighbor distances, it is conceivable that other functional forms can lead to similar or even better results than R-Exp. To gauge the importance of that choice, we also consider Gaussian repulsion

$$V_{\mathrm{R}}(r) = V_0 \sum_j \exp\left\{-r^2/\left(2\sigma_{\mathrm{R}}^2\right)\right\}^2 \qquad \text{(R-Gauss)}. \tag{18}$$

In their original work on EAM, Daw *et al.* [3] followed the argument that the dominant contribution to repulsion at very small distances originates from Coulomb

repulsion between the ions that is increasingly screened as the ions moved apart. This lead them to use a screened Coulomb repulsion of the form

$$V_{\mathrm{R}}(r_{ij}) = \frac{1}{4\pi\epsilon_0}\frac{Q^2(r_{ij})}{r_{ij}}, \qquad \text{(R-SC)} \tag{19}$$

where $Q(r_{ij})$ is an effective charge obeying

$$Q(r_{ij}) = Q_0(1 + r_{ij}^2/r_{\mathrm{c}}^2)e^{-r_{ij}/\sigma_{\mathrm{R}}}. \tag{20}$$

Here r_{c} is another adjustable parameter, which is of similar magnitude as the radius of the core shells.

In the later construction of the MEAM potential, Baskes followed yet another path. [38] He argued that the two-body repulsion should be independent of the structure, and that it can therefore be determined, for a given embedding function, from the EOS, e.g., from the EOS of fcc Cu via

$$V_{\mathrm{R}}\,(a) = \frac{2}{Z_{\mathrm{fcc}}}\left[E_{\mathrm{fcc}}(a) - F\left\{\rho_{\mathrm{fcc}}(a)\right\}\right] \text{ (R-EOS)}, \tag{21}$$

where a refers again to the nearest-neighbor distance and $Z_{\mathrm{fcc}} = 12$ is the coordination number in a fcc crystal. Using this procedure, $F(\rho)$ cannot be determined simultaneously from the EOS via equation (13).

2.2. Systematically modified embedded-atom potentials

In this section, we undertake a slightly altered and more systematic modification of the embedded-atom method (SMEAM) than the ones commonly pursued. Our generalization is based on assumptions that are similar in spirit as a systematic expansion in terms of coordinate-dependent two-body, three-body, and higher-order many-body interactions. [46] However, rather than coordinates, we use the charge density $\rho_i(\mathbf{r}_i)$ along with its higher-order derivatives as the natural variables of the embedding energy as proposed in the pioneering work on the quasi-atom method. [20] A systematic expansion should be possible, as knowing $\rho_i(\mathbf{r})$ together with its higher-order derivatives allows one, in principle, to reconstruct the positions of all atoms other than atom i already in place. For the reconstruction to be unique, each (neutral) atom or element only needs to be assigned its own characteristic charge density $f_j(r)$. Similar argument might also apply to coarse-graining in other systems and for example allow one to go beyond conventional density-based approaches [47] in soft-matter systems. From this phenomenological point of view, it is not clear how the embedding energy should depend on density and its derivatives, beyond restrictions imposed by symmetry. It is not clear either if or how rapidly the expansion converges. It is nevertheless worth exploring if well-motivated choices improve results with respect to EAM potentials assuming uniform densities at the embedding site. A first step in that direction was taken by Wu *et al.*: [48] They demonstrated that a density-gradient-corrected EAM potential enhanced the simultaneous description of dimer, bulk, and surface properties of aluminum. However, the expansion was truncated after the square-gradient density.

Note that C-MEAM already contains the envisioned expansion in an asymptotic limit: If all coefficients $\sigma_{\mathrm{Q}n}$ in equation (12) are assigned the same value σ_{Q} and σ_{Q} is small compared to nearest-neighbor distances, then the $\rho_{i\alpha_1,\ldots,\alpha_n}$ are the n-th order derivative up to a factor σ_{Q}^n. Assuming the coefficients $c_{\mathrm{G}2},\ldots,c_{\mathrm{T}2}$ to be small, the C-MEAM based embedding function can be expanded to leading order as

$$F\left(\rho_i^{(g)}\right) = F(\rho_i) + \rho_i F'(\rho_i)\left(2c_{\mathrm{G}2}\frac{\rho_{i\alpha}^2}{\rho_i^2} + 2c_{\mathrm{H}2'}\frac{\rho_{i\alpha\beta}^2}{\rho_i^2} + 2c_{\mathrm{T}2}\frac{\rho_{i\alpha\beta\gamma}^2}{\rho_i^2}\right) + \ldots \quad (22)$$

For a Friedel embedding function, this can be cast in the appealing form

$$F(\rho_i,\rho_{i\alpha},\rho_{i\alpha\beta},\ldots) = A\sqrt{\rho_i}\left(1 + c_{\mathrm{G}2}\frac{\rho_{i\alpha}^2}{\rho_i^2} + c_{\mathrm{H}2'}\frac{\rho_{i\alpha\beta}^2}{\rho_i^2} + c_{\mathrm{T}2}\frac{\rho_{i\alpha\beta\gamma}^2}{\rho_i^2}\right) + \ldots \quad (23)$$

Corrections to the EAM energy, as those just derived, must contain the correct symmetry, i.e, they must be invariant under rotation and mirror reflection. While the MEAM correction obeys these symmetries, additional terms are allowed. They can be grouped according to the number of indices needed to form a specific invariant. For example, a missing invariant is $\rho_{i\alpha\alpha}$. Since the square gradient (SG) $\rho_{i\alpha}^2$ and $\rho_{i\alpha\alpha}$, which contains amongst other terms the trace of the Hessian (H) of the embedding density, are the only invariants formed by one pair of indices, the most general linear correction of this rank is

$$\Delta F_1(\rho_i) = C_{\mathrm{SG}}(\rho_i)\rho_{i\alpha}^2 + C_{\mathrm{H}}(\rho_i)\rho_{i\alpha\alpha}. \quad (24)$$

Note that the prefactors, $C_{\mathrm{SG}}(\rho_i)$ and $C_{\mathrm{H}}(\rho_i)$ generally are functions of density as can be seen from equation (23), for which one would find $C_{\mathrm{SG}}(\rho_i) = Ac_{\mathrm{SG}}/\rho_i^{3/2}$.

The next group of terms in SMEAM contains all invariants formed by two pairs of indices. (Indices always have to come in pairs, because otherwise the contraction of the expressions to a scalar would not be complete and mirror symmetry would be violated.) This leads to the two-index-pair energy correction

$$\begin{aligned}\Delta F_2 = {} & C_{\mathrm{SG}2}\rho_{i\alpha}^2\rho_{i\beta}^2 + C_{\mathrm{SGH}}\rho_{i\alpha}^2\rho_{i\beta\beta} + C_{\mathrm{SGH}'}\rho_{i\alpha}\rho_{i\beta}\rho_{i\alpha\beta} + C_{\mathrm{GT}}\rho_{i\alpha}\rho_{i\alpha\beta\beta} \\ & + C_{\mathrm{H}2}\rho_{i\alpha\alpha}\rho_{i\beta\beta} + C_{\mathrm{H}2'}\rho_{i\alpha\beta}\rho_{i\alpha\beta} + C_{\mathrm{F}}\rho_{i\alpha\alpha\beta\beta}, \end{aligned} \quad (25)$$

which consists of seven summands. Here, the prefactors, $C_{\mathrm{SG}2},\ldots,C_{\mathrm{F}}$, are again assumed to depend on density, in the most general case. (The index GT in C_{GT} relates to a coupling of the gradient to a tensor of rank three, while F in C_{F} stands for the contraction of a tensor of rank four.) It later turns out that not all the invariants substantially improve the description of our selection of copper structures. However, from a symmetry point of view, it is not clear which invariants should be included and which ones can be left out. This can be seen from an analogy to linear elasticity: in linear elasticity, one also contracts the product of a rank two tensor to yield an energy in the same fashion as in the terms proportional to $C_{\mathrm{H}2}$ and $C_{\mathrm{H}2'}$. In this analogy, the prefactors $C_{\mathrm{H}2}$ and $C_{\mathrm{H}2'}$ would correspond to the two independent Lamé coefficients and their ratio should not simply be assigned *ad-hoc*.

Higher-order terms in our expansion can be constructed systematically from the invariants of (commutative) tensor products $\rho_i(l_1)\otimes\rho_i(l_2)\cdots\otimes\rho_i(l_k)$, where the elements

of $\rho_i(l)$ are defined in analogy to those in equations (9)–(11). Unfortunately, the number of resulting invariants quickly rises with the order of the tensor: we count 11 tensors with three pairs of indices having 20 independent invariants total. It is not obvious why $\rho^2_{i\alpha\beta\gamma}$ should be the most important one out of these 20 independent invariants. In fact, for copper we find the term $\rho^2_{i\alpha}\rho^2_{i\beta}\rho^2_{i\gamma}$ to be the most important out of the tested invariants based on three pairs of indices.

In order to obtain a more intuitive understanding of SMEAM, it may be beneficial to express some of the expansion summands in terms of bond angles. The easiest-to-interpret summands are formed by integer powers of the square gradient, i.e., $\rho^2_{i\alpha_1}\cdot\ldots\cdot\rho^2_{i\alpha_n}$. The square-gradient expression can be written as

$$\rho^2_{i\alpha} = \sum_j n^\alpha_{ij} f_j(r_{ij}) \sum_k n^\alpha_{ik} f_k(r_{ik}) \tag{26}$$

$$= \sum_{jk} \cos\gamma_{ijk}\, f_j(r_{ij}) f_k(r_{ik}) \tag{27}$$

$$\approx \sum_{j,k\in\text{n.n.}} \cos\gamma_{ijk}\, f^2_j(a) \qquad \text{(identical distance } a \text{ for all n.n.)}, \tag{28}$$

where γ_{ijk} refers to the bond angle formed by the atoms i, j, k on atom i. In the approximation (28), we restricted the sum to the dominant nearest-neighbor (n.n.) shell. Raising the square-gradient expression to the n-th power then leads to summands linear in $(\cos\gamma_{ijk})^n$, that is, to terms proportional to $\cos(n\gamma_{ijk})$ and related expressions of $2\pi/n$ symmetry. Thus, the coefficients in front of the integer powers of the square gradient effectively determine an environment-dependent bond-angle potential. If we chose the embedding energy to be linear in ρ, the pertinent expressions would reduce to more conventional bond-angle potentials.

As an additional example for an invariant in a SMEAM expansion, we consider $\rho_{i\alpha\beta}\rho_{i\alpha}\rho_{i\beta}$. Proceeding in the same fashion as above, we obtain

$$\rho_{i\alpha\beta}\rho_{i\alpha}\rho_{i\beta} = \sum_{jkl} \cos\gamma_{ijk}\cos\gamma_{ijl}\, f(r_{ij}) f(r_{ik}) f(r_{il}). \tag{29}$$

The prefactor to this expression in the SMEAM expansion, $C_{SGH'}$, thus couples bond angles on a given atom and thereby "renormalizes" the effective bond-angle potential. If $F(\rho)$ were linear in ρ, the resulting SMEAM summand would correspond to a four-body interaction. Other couplings can be interpreted similarly. It can then be seen that contractions of $\rho_i(l_1)\otimes\rho_i(l_2)\cdots\otimes\rho_i(l_k)$ relate to effective $(k+1)$-body potentials plus higher-order interactions.

Discussing all implications of the SMEAM expansion including further generalizations, such as a coupling of the density and its derivatives on different atoms, is beyond the scope of this study. It shall suffice to state that the choice of the prefactors of the invariants determines the equilibrium structures and their compliance. For example, a negative prefactor to the square-gradient invariant would favor large gradients and thereby bias the system towards structures missing inversion symmetry. Other invariants can lead to other ways in which closed-packed structures are destabilized,

e.g., a positive prefactor to the invariant $\rho^2_{i\alpha\beta}$ favors low-dimensional structures, as we demonstrate in section 3.

We conclude this section with some technical comments including how the evaluation of invariants can be coded with little numerical overhead. Most importantly, all calculations in this work were conducted assuming that the $\rho_{i\alpha_1,\ldots,\alpha_n}$ are proportional to $\sum_j n_{\alpha_1} \ldots n_{\alpha_n} \exp(-r_{ij}/\sigma_\mathrm{Q})$. This is not a serious approximation, amongst other reasons because the nearest-neighbor distances turn out five times greater than σ_Q. At the same time, coding and computing time for the evaluation of the invariants is reduced substantially.

To generate low-order tensors $\rho_{i\alpha_1,\ldots,\alpha_n}$ only few extra floating point operations are needed. To compute the gradient term, three multiplications are needed for each neighbor of the central atom. The next-rank tensor has six independent components, each of which needs two multiplications. It continues with ten (fifteen) components for the tensor of rank three (four). This effort needs to be compared to taking a square-root and an exponential of r^2_{ij}, which each by itself costs substantially more than a simple multiplication. Most importantly, the numerical effort is linear in the number of neighbors of the central atom. In most cases, at least for condensed-matter systems, where each atom interacts with a few dozen neighbors, the evaluation of the invariants adds only a small amount of extra CPU time. For example, once $\rho_{i\alpha\beta\gamma}$ is known, the invariant $\rho^2_{i\alpha\beta\gamma}$ can be coded as twelve multiplications and nine additions.

2.3. Simple analytical considerations on the Gupta potential

As mentioned before, Gupta designed a simple EAM potential by combining the components C-Exp, E-Friedel, and R-Exp. A great advantage of simple functional forms is that they allow one to conduct analytical calculations by hand so that trends can be ascertained. This section presents such calculations, in which the parameters V_R, σ_R, A, and σ_Q are the only parameters. Since two parameters can be used to define the units of energy and length, the Gupta potential is described by only two non-dimensional coefficients.

Assuming that both σ_Q and σ_R are much less than the difference between next-nearest neighbor and nearest-neighbor distances, which holds for all our investigated structures except bcc, one can approximate the total energy of a structure with

$$V(Z,a) \approx \frac{ZV_\mathrm{R}}{2} \exp\left(-\frac{a}{\sigma_\mathrm{R}}\right) + A\sqrt{Z \exp\left(-\frac{a}{\sigma_\mathrm{Q}}\right)}, \tag{30}$$

where a is the bond length and Z the coordination number of a central atom. For this potential, it is easily possible to estimate the equilibrium bond length a_0 by minimizing $V(a)$ with respect to a. Doing so leads to

$$a_0 \approx \frac{2\sigma_\mathrm{Q}\sigma_\mathrm{R}}{2\sigma_\mathrm{Q} - \sigma_\mathrm{R}} \ln\left(-\sqrt{Z}\,\frac{\sigma_\mathrm{Q}V_\mathrm{R}}{\sigma_\mathrm{R}A}\right), \tag{31}$$

i.e., the bond length increases roughly logarithmically with increasing coordination.

Substituting this expression back into equation (30) reveals that both terms contributing to the total potential scale according to

$$V(Z, a_0) \propto Z^{\mu} \tag{32}$$

and

$$\mu = \frac{\sigma_{\mathrm{Q}} - \sigma_{\mathrm{R}}}{2\sigma_{\mathrm{Q}} - \sigma_{\mathrm{R}}}. \tag{33}$$

Thus, in the limit of $\sigma_{\mathrm{Q}} \gg \sigma_{\mathrm{R}}$, the binding energy $E_0 = V(Z, a_0) \propto \sqrt{Z}$. In reality, this limit is not exactly satisfied so that one could expect effective values for μ to be less than 1/2. However, including next-nearest neighbors counteracts this correction so that one can take $E_0 \propto \sqrt{Z}$ as a zero-order approximation for binding energies.

We note in passing that in order for dimers to be stable and meaningful, parameterizations need to satisfy, $A < 0$, $2\sigma_{\mathrm{Q}} > \sigma_{\mathrm{R}}$ (attractive contribution dominates at large distances), and $V_{\mathrm{R}} > -A$ (positive energy in the limit where two atoms have identical coordinates). This implies that for $\sigma_{\mathrm{Q}} < \sigma_{\mathrm{R}} < 2\sigma_{\mathrm{Q}}$, our back-of-the-envelope calculation predicts the formation of one-coordinated structures to be favorable. For $\sigma_{\mathrm{R}} < \sigma_{\mathrm{Q}}$ large coordination will be preferred. It will thus be difficult for a Gupta potential missing gradient and related corrections to make structures of medium coordination to be the ground state, unless the next-nearest neighbor contributions become large, or, the charge density gradients and higher-order derivatives start to play a role. This is discussed in more detail in section 3, see also equation (39).

2.4. Investigated Structures

To study the transferability of the investigated potentials between different geometries, we consider a variety of structures ranging from clusters via chains and sheets or tilings to bulk solids. In the selected geometries, all atoms are equivalent by symmetry so that charge (and spin) transfer is suppressed, unless the electronic structure spontaneously breaks the symmetry. Some of the investigated geometries represent stable or at least close-to-metastable structures, while others are purely hypothetical. Those are nevertheless included into our test to get an idea about the differences between classical and quantum models far from mechanical equilibrium. Small, highly-symmetric Cu clusters, as the ones described hereafter, typically undergo a Jahn–Teller deformation to remove the degeneracy of their highest occupied molecular orbital with the lowest unoccupied orbital. Mimicking this effect is outside the scope of the conventional EAM formulation, which is why we purposefully ignore such structures.

As zero-dimensional objects, we chose the dimer ($Z = 1$), the equilateral triangle ($Z = 2$), the square ($Z = 4$), and in addition all Platonic solids. The latter are the tetrahedron, the cube, and the dodecahedron, each having a coordination number of $Z = 3$, the octahedron ($Z = 4$), and the icosahedron ($Z = 5$). We furthermore added the cuboctahedron, which is an Archimedean body with $Z = 4$. Our one-dimensional objects consist of the linear chain ($Z = 2$), the square ladder ($Z = 3$), and a triangular strip ($Z = 4$), which can be obtained from the latter (ladder) by shearing the

structure appropriately. The considered two-dimensional structures are the honeycomb or hexagonal lattice ($Z = 3$), the square lattice ($Z = 4$) as well as the kagome tiling ($Z = 4$) and the triangular tiling ($Z = 6$). Bulk solids are the unstable diamond ($Z = 4$) and simple cubic ($Z = 6$) crystals, fcc and hexagonal close packed (hcp), each having $Z = 12$. In addition, we consider the body-centered cubic (bcc) crystal, which is stable at high temperature and, rigorously speaking, has $Z = 8$. However, the six next-nearest neighbors are only 15% more distant from a central atom than the nearest-neighbors, so that one could also argue that bcc has a coordination number of $Z = 14$, or any number in between 8 and 14. In all other cases than bcc, there is at least a 40% increase in spacing from nearest to next-nearest neighbors. This difference then clearly exceeds some pertinent force-field parameters such as σ_{Q} in equation (5) or σ_{R} in equation (17). Consequently, the coordination number is reasonably well defined for any investigated structure other than bcc.

2.5. Observables and χ^2 goodness

Force fields are typically fitted to a small set of target observables or reference quantities. As the set of systems in our study covers a wide variety of geometries, we use characteristics which can be defined for the whole set: the equilibrium nearest-neighbor distance a_0, the equilibrium energy per atom E_0, and the "stiffness" S defined as

$$S = \left.\frac{\partial^2 E_0(a)}{\partial a^2}\right|_{a=a_0}. \tag{34}$$

Given the atomic packing fraction of a particular crystal, the bulk modulus B can be deduced from S and a_0 in a straightforward fashion. Thus, when fitting to a_0, E_0, and S, we implicitly fit to B. For two- and three-dimensional structures, elastic tensor elements can be defined containing information on the compliance of the system in addition to that contained in the bulk modulus. These elements are C_{11}, C_{12}, and C_{44} for isotropic systems or crystals of cubic symmetry. We never used target values for those numbers while optimizing the adjustable force-field parameters, and instead tested later if their values were reproduced. In fact, we did not compare the various C_{ij} directly but indirectly via two dimensionless numbers. These were a measure $\tilde{C}_{\mathrm{Cauchy}}$ for the violation of the Cauchy relation, $C_{12} = C_{44}$,

$$\tilde{C}_{\mathrm{Cauchy}} = \frac{C_{12} - C_{44}}{C_{11}} \tag{35}$$

and a measure $\tilde{C}_{\mathrm{iso}}$ for the violation of the isotropy condition, $C_{44} = (C_{11} - C_{12})/2$,

$$\tilde{C}_{\mathrm{iso}} = \frac{C_{44} - (C_{11} - C_{12})/2}{C_{11}}. \tag{36}$$

The quality of a fit is commonly measured with a χ^2 penalty function

$$\chi^2 = \frac{1}{\sum_i w_i} \sum_i w_i \left(\frac{O_i^{\mathrm{EAM}} - O_i^{\mathrm{DFT}}}{\Delta O_i} \right)^2, \tag{37}$$

where O_i^{DFT} and O_i^{EAM} are the values of a given observable as deduced from DFT and EAM, respectively. ΔO_i is an error that we perceive as "small" but achievable for a good force field, while w_i is a weight with which each observable enters the fit. Thus, a value of $\chi^2 = 1$ for a given subset of data is seen as satisfactory, as it indicates that deviations were within expectations. As default values for the relative uncertainties $\Delta O/O_{\mathrm{DFT}}$, we use 0.01 for a_0, 0.05 for E_0, and 0.15 for S.

Adjustable force field parameters were optimised for our chosen χ^2 function using a standard simulated annealing procedure, which was coded in C++. We chose simulated annealing to identify possible multiple minima on the χ^2 surface. Its slow convergence to a minimum was not seen as an impediment, because the set of the selected properties can be computed 1,000 times per second on a single core.

2.6. DFT calculations

This study is conducted in the spirit that the DFT data describes a fictional material and that we investigate how well the produced data can be modeled by a classical force field. Thus, it is of higher priority to produce a set of data that is as self-consistent as possible than to generate data that is as accurate as possible for a given structure. This is why we model all structures with identical methods instead of employing different methods for different structures. In addition, we purposefully ignore or suppress effects that cannot be described by simple EAM potentials even if they can or do occur in real systems, such as Jahn–Teller distortions or spin-frustrated structures in lower-dimensional systems.

We nonetheless try to evaluate the quality of the data. For this purpose, direct comparison to experiment can only be made for fcc copper and the copper dimer. Other solid structures are not stable at ambient pressure and low temperatures, except for hcp, which, however, is very similar to fcc, so that no substantially new information is gained. Likewise, the one and two-dimensional crystals cannot be prepared in the laboratory, because real clusters tend to have smaller symmetry than those selected by us. To obtain a rough estimate for the accuracy of the DFT target numbers, we employ three different DFT methods and compare the results to each other.

All three sets of pseudopotential calculations were performed with the Quantum Espresso software suite. [49] All calculations approximated the exchange-correlation functional with Perdew–Burke–Ernzerhof (PBE) model. [50, 51] One set of calculations is based on the Hartwigsen–Goedecker–Hutter (HGH) normconserving pseudopotential whose results are also used as our reference data. [52] The other two calculations used the Kresse-Joubert projector-augmented plane-wave method (KJPAW) [53] and the ultrasoft Rappe-Rabe-Kaxiras-Joannopoulos pseudopotential (RRKJUS). [54] The HGH and RRKJUS calculations included a semicore state d in the valence.

All calculations of infinite structures were done on a grid with 16 k-points in each periodic direction. For low-dimensional systems, the calculations were done in a sandwich geometry at the gamma point. The width of the cell in the "vacuum direction" was 36-44 Å. For clusters and monomers, we also employed the Martyna-Tuckerman

correction [55] although it turned out that this did not change the significant digits of our results. For the normconserving HGH calculations we used a plane-wave kinetic energy cut-off of 200 Ryd, KJPAW and RRKJUS calculations were both done with cut-off 65 Ryd. The electronic density cut-off equalled four times the plane-wave cut-off.

The cohesive energies were obtained as differences to the energy of an isolated monomer, which for the HGH method were computed as described above for the clusters, and in the other cases the value provided with the potential was used. The stiffnesses were calculated from the coefficients of a third order polynomial fit to at least five datapoints within a few per cent from the nearest neighbor distance corresponding to the minimum energy. Calculations were not spin polarised for the above-mentioned reason that this effect is beyond the scope of the tested force fields.

3. Results

3.1. DFT results

In this section, we summarize our DFT results for the investigated structures. We present the PBE data in graphical forms rather than in tables, because this facilitates their interpretation. Figure 1 supports the back-of-the envelope calculation presented in section 2.3 of a nearest-neighbor spacing that increases roughly logarithmically with the coordination number. For fcc, the lattice constants from all three methods are 3.65–3.66 Å and agree reasonably well with the experimental value 3.615 Å. [56, 7, 8] All three methods put the dimer length between 2.23 Å and 2.27 Å, which is in decent agreement with the literature value of 2.2197 Å. [57] Deviations from the predicted trend are such that the DFT-based bond lengths are smaller for all low-dimensional structures having inversion symmetry but also for the hypothetical or metastable diamond and simple cubic lattices.

The prediction that the binding energy roughly follows a power law also turns out correct, as can be seen in figure 2. The relative scatter in the binding energies is larger than for the lattice constants but trends are consistent. The fcc binding energies of the HGH and RRKJUS methods are in good agreement with the experimental value of $567.18 \cdot 10^{-21}$ J, [58, 59, 60, 61] while KJPAW slightly overestimates it. The dimer energy 192×10^{-21} J is also in reasonable agreement with the literature value of $\sim 170 \times 10^{-21}$ J. As for the fcc structure, the highest and lowest values are given by the HGH and KJPAW methods, respectively, the difference being roughly 22×10^{-21} J. Structures leading to energies above (below) the line extrapolating the behavior between the two extremes — dimer on one end and fcc on the other end — result in bond lengths below (above) the corresponding line for the nearest-neighbor spacing. These trends have certainly been known for a long time [62] but have not been investigated systematically in terms of EAM potentials. From the line connecting the $Z = 1$ and the $Z = 12$ structures, one can read off an exponent of $\mu \approx 0.405$ in equation (32) and thus, using equation (33), one may conclude that the ratio $\sigma_{\mathrm{R}}/\sigma_{\mathrm{Q}}$ should not be too far from 1/3.

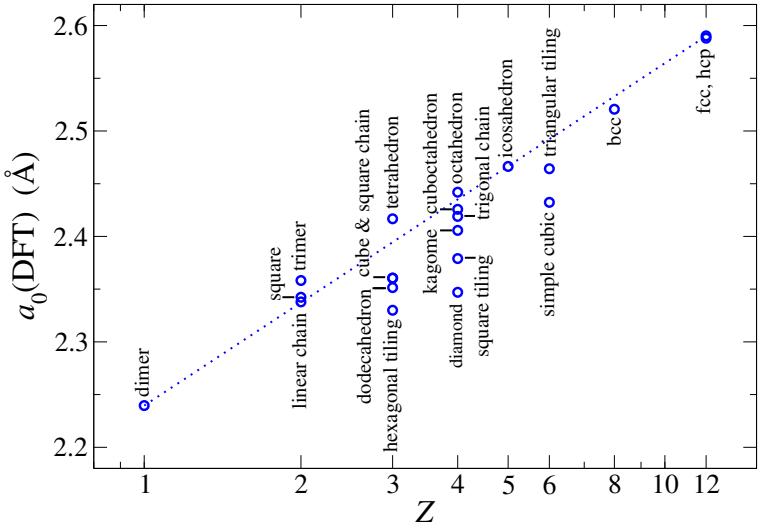

Figure 1. DFT results for the equilibrium Cu-Cu bond length a_0 as a function of the coordination number Z for different geometries.

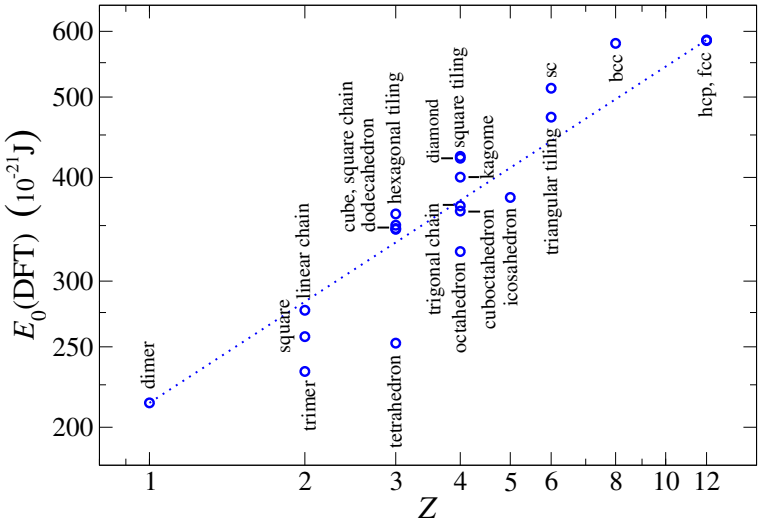

Figure 2. DFT results for the binding energy E_0 as a function of the coordination number Z for different geometries. The dotted line connects the DFT results for the highest and the lowest binding energy. It corresponds to a Z^μ power law with an exponent $\mu \approx 0.405$.

The stiffnesses shown in figure 3 follow a similar power law as the binding energies. This can be rationalized by extending the calculations presented in section 2.3 to elastic moduli: energies and stiffnesses turn out proportional to each other, $2\sigma_Q\sigma_R$ being the proportionality constant. The *ab initio* results for the stiffnesses S and elastic moduli C_{11}, C_{12} and C_{44} are again in good agreement with the values calculated from the experimentally known moduli of fcc, $S \sim 2309$ GPa·Å, $C_{11} \sim 176$ GPa, $C_{12} \sim 124$ GPa and 82 GPa. [63, 56] The dimer stiffness 648 GPa·Å is also close to the value 640 GPaÅ,

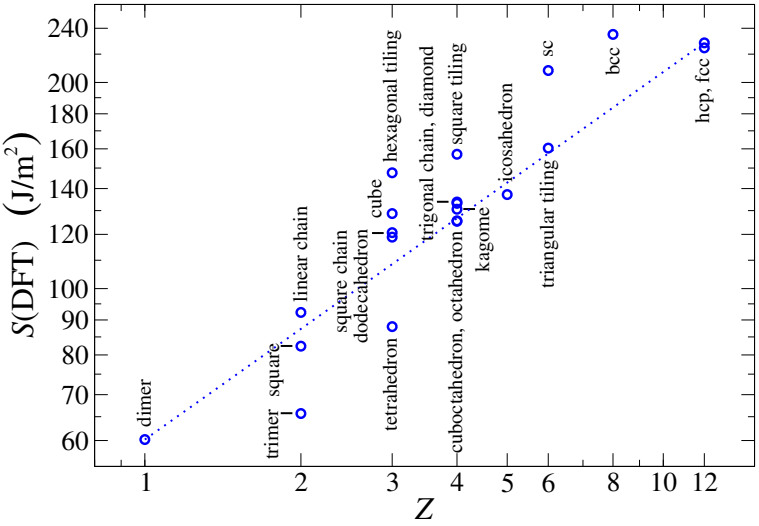

Figure 3. DFT results for the stiffness $S = \partial^2 E_0/\partial a_0^2$ as a function of the coordination number Z for different geometries. The dotted line connects the DFT results for the highest and the lowest stiffness.

which can be deduced from the literature. [57]

Between different DFT approaches, we find typical deviations of the bond lengths, the binding energies, and the stiffnesses to be of order O(1%), O(5%), and O(15%), respectively, when averaged over all structures, each structure being given identical weight. For bond lengths and binding energies deviations are systematic and not very scattered, while differences in stiffness show no obvious trends. Since one cannot expect force fields to surpass the accuracy of DFT calculation, we define the description of the data as satisfactory if the deviation between the force-field based numbers and the HGH results are of similar magnitude as the deviation between different DFT methods. This motivated our choice to use $\Delta a/a = 0.01$, $\Delta E_0/E_0 = 0.05$, and $\Delta S/S = 0.15$ for the evaluation of the χ^2 goodness function. With this choice, we label a value of $\chi = 1$ as satisfactory.

3.2. Results for the Gupta potential

We start the presentation of our results on conventional (in the sense of uniform-density approximation) EAM potentials with the analysis of the Gupta potential. As we discuss in more detail further below, these results are representative for other conventional EAM potentials. For our reference data, we found the original parametrisation to be somewhat unfavorable and thus refitted the four adjustable parameters to our DFT data. The obtained numbers were $V_{\mathrm{R}} = 1.55971\times10^{-15}$ J, $a_{\mathrm{R}} = 0.22839$ Å, $A = -1.31838\times10^{-18}$ J, and finally $a_{\mathrm{Q}} = 0.64039$ Å.

The new set of parameters reduced the square root of our default goodness function from $\chi = 8.988$ to $\chi = 0.6741$. Thus, the quality of the data for lattice constants, binding energies, and stiffnesses were within the expectations. Despite this level of agreement,

it is instructive to investigate deviations between the EAM and the DFT results.

Figure 4 reveals that most EAM lattice constants are within 1% accuracy. As such, the observation of $a_0(Z) - a_0(1) \approx \ln(Z)$ is reproduced. However, for a fixed value of Z, one can observe that EAM bond lengths for bulk structures are systematically too large while those for structures with $Z \leq 3$ tend to be too small.

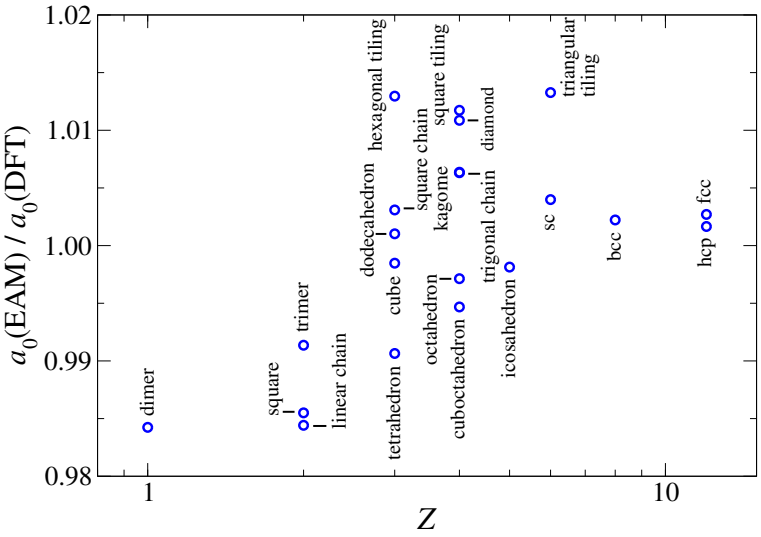

Figure 4. EAM equilibrium length a_0(EAM) divided by the DFT equilibrium length a_0(DFT) as a function of the coordination number Z for different geometries.

Binding energies deduced from a reparametrised Gupta potential also reproduce the predicted power law dependence from section 2.3 quite well, as shown in figure 5. However, in comparison to the DFT data presented in figure 2, the fluctuations in the Gupta E_0 for a fixed value of Z are rather small. Even worse, they often convey the wrong order for a fixed value of Z. For example, the two-dimensional tilings are predicted to have relatively small binding energies, while DFT calculations find them to be largest. This trend is observed by *all* EAM potentials, as long as they do not have C-MEAM or SMEAM corrections. This can be easily rationalised: In conventional EAM potentials, the first correction to the calculations presented in section 2.3 comes from the second neighbor shell. The only information relevant to EAM then is how distant the second shell is and how many atoms sit on it, while bond angles do not play a role. As a consequence, EAM cannot reproduce the observation that DFT tends to prefer open structures over densely-packed geometries, sometimes even at the expense of reducing coordination. For example, unlike EAM, DFT finds that the linear chain with $Z = 2$ is clearly more stable than the tetrahedron ($Z = 3$) and the hexagonal tiling ($Z = 3$) has distinctly greater binding energy than the octahedron with $Z = 4$. Similar statements do not only hold for the Gupta potential but for any of the tested conventional EAM potentials.

The results on the stiffness of the structures, see figure 6, are only semi satisfactory. While absolute errors of less than 30% can be considered to be reasonable, there seems to

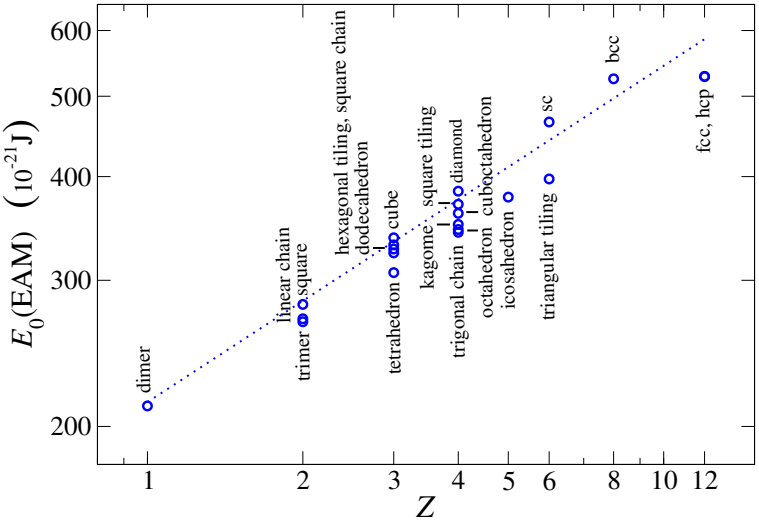

Figure 5. EAM results for the binding energy E_0(EAM) as a function of the coordination number Z for different geometries. The dotted line is identical to that drawn in figure 2.

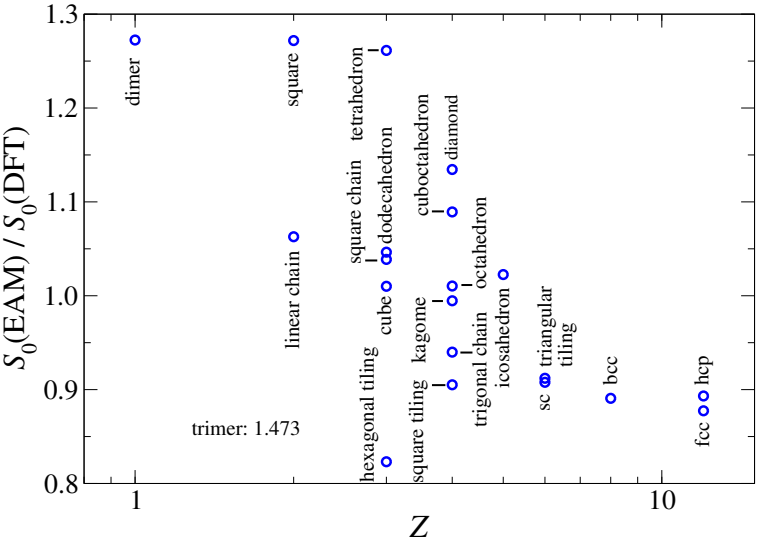

Figure 6. EAM equilibrium stiffness S_0(EAM) divided by the DFT stiffness S_0(DFT) as a function of the coordination number Z for different geometries.

be a systematic deviation: Stiffnesses are overestimated for $Z < 3$ and underestimated for $Z > 5$.

3.3. Conventional EAM methods

As stated in the previous section, the reparametrised Gupta potential reproduces the data with a $\chi(\mathrm{C-Exp}, \mathrm{E-Friedel}, \mathrm{R-Exp})$ of ≈ 0.6741. In this section, we explore by how much the agreement with the target DFT data can be improved within the

context of conventional EAM methods, i.e., those in which no (effective) gradients are taken, such as in MEAM or SMEAM.

If we keep the R-Exp as repulsion and E-Friedel as embedding function, the following goodness is obtained for the different charge schemes, when re-optimizing each parameter of the full potential $\chi(\mathrm{C-DG}) = 0.8892$, $\chi(\mathrm{C-Gauss}) = 0.7790$, and $\chi(\mathrm{C-IM}) = 0.6500$. These results suggest that elaborate tables for the charge density or the the evaluation of complicated functions do not benefit EAM calculations more than a simple exponentially decaying charge density, at least not in the context of a conventional EAM method.

We next change the embedding function while keeping R-Exp as repulsion and C-Exp as charge density. This yielded $\chi(\mathrm{E\text{-}MEAM}) = 0.9201$ and $\chi(\mathrm{E\text{-}Taylor}) = 1.1703$ using four terms in the polynomial fit. The latter fit turned out to converge very slowly without leading to better minima of the goodness function than our default choice E-Friedel, which only needs one instead of four parameters. The results for E-EOS depend on the nature of the EOS. For Birch–Murnaghan (BM), we found the best value of $\chi(\mathrm{E-EOS-BM}) = 0.5748$, while Rose-Vinét (RV) only lead to $\chi(\mathrm{E-EOS-RV}) = 0.7542$. The improvement of the E-EOS-BM embedding function over a simple square-root function is so small that we nevertheless consider E-Friedel more appealing.

The last test in this section relates to the repulsion, which we change while using C-Exp for the charge density and E-Friedel as embedding function. We find $\chi(\mathrm{R-Gauss}) = 0.6918$ and $\chi(\mathrm{R-SC}) = 0.6742$ while the two EOS-based approaches yield $\chi(\mathrm{R-EOS-BM}) = 0.8119$ and $\chi(\mathrm{R-EOS-RV}) = 0.8422$. Again, no significant improvement can be found over the simple exponential term. Even if one of the two R-EOS methods had given a better value, designing the repulsive potential from the EOS would have been unsatifactory whenever first- and second-nearest neighbors cannot be clearly distinguished.

We note that for *any* EAM assuming the uniform density approximation, the spread of binding energies was relatively small for a fixed number of nearest neighbors Z compared to DFT. The errors were systematically largest for the tetrahedron, hexagonal and triangular tilings. Moreover, all conventional EAM potentials give a very small relative difference in hcp and fcc binding energies, and in most cases mispredict its sign. The $O(0.03\%)$ EAM energy difference between fcc and hcp originates from the third and fourth neighbor shells. Yet, DFT gives a ten times greater value for the hcp–fcc binding energy difference, (0.3%), which compares well with experimental results. [64, 65, 66, 67] Quantum-chemical arguments relate the hcp-fcc energy difference to geometric effects in the first-neighbor shells of the structures. [68, 69, 70] Representing such effects for fcc versus hcp is beyond the feasibility of conventional EAM potentials. Since we are looking for an expression which can be improved by adding in the physically meaningful missing terms, getting the right value by modifying the long-range part of the potential would be counter-productive. Similar comments are certainly valid for other structures as well. Thus, correcting the sequence of binding energies for a given value of Z in a

physically meaningful fashion seems to be outside the reach of conventional EAM.

In the context of SMEAM, the invariant $\rho_{i\alpha\alpha\beta\beta}$ is the lowest-order invariant yielding different nearest-neighbor values for fcc and hcp, allowing to represent the energy difference of the two structures as a geometric effect. This is similar to the way how a six'th order moment expansion for bond-order potentials [71] makes it possible to distinguish the energy difference between hcp and fcc.

3.4. Modified EAM potentials

In this section, we discuss results on the following modified EAM potentials: (i) the original MEAM with original parameters, (ii) the original MEAM with parameters that were optimised for our learning set, (iii) the Gupta potential plus a square-gradient correction, (iv) SMEAM as defined in section 2.2, see also equation (38), and (v) a hybrid of Gupta, MEAM, and SMEAM, for which we use an effictive charge density, as defined in C-MEAM (plus additional terms), and insert it into E-Friedel, while keeping R-Exp as repulsion. The embedding energy of the last variant is obtained when pulling the last factor on the r.h.s. of equation (38) under the square root. In all cases but (i), no nearest-neighbor cutoffs were employed for any quantity. Instead, any R_c was set greater than $8\sigma_\mathrm{Q}$.

For the goodness function, we obtained $\chi(\mathrm{i}) = 1.950$, $\chi(\mathrm{ii}) = 0.6468$, $\chi(\mathrm{iii}) = 0.4554$, $\chi(\mathrm{iv}) = 0.3346$ and $\chi(\mathrm{v}) = 0.3642$. Thus, it appears that a systematic expansion based on simple analytical expressions is the most accurate choice for our learning set of structure encompassing many different local binding environments. However, as before, trends regarding bond lengths, binding energies, and stiffnesses, are similar for different EAM modifications. Since SMEAM gives the best results, we focus our discussion on that approach.

While fitting SMEAM, we noticed that only few invariants are needed to optimize the goodness function. The final expression for the embedding energy reads

$$F(\rho, \rho_\alpha, ...) = A\sqrt{\rho}\left(1 + c_{\mathrm{SG2}}\frac{\rho_{i\alpha}^2}{\rho^2} + c_{\mathrm{H2'}}\frac{\rho_{i\alpha\beta}^2}{\rho^2} + c_{\mathrm{SG6}}\frac{\rho_{i\alpha}^2}{\rho^2}\frac{\rho_{i\beta}^2}{\rho^2}\frac{\rho_{i\gamma}^2}{\rho^2}\right). \tag{38}$$

None of the additional low-order invariants we tested reduced the goodness function by more than fractions of a per cent, even when combining several of them, while leaving out any of the listed invariants noticeably increased χ. Note that c_{SG2} and related coefficients in equation (38) are dimensionless, unlike the functions $C_{\mathrm{SG2}}(\rho)$ in the prefactors on the r.h.s. in equation (25). This is because $\rho_{i\alpha}$ is not the α component of the gradient of the charge density but σ_Q times $\partial_\alpha\rho$.

Figure 7 shows that SMEAM bond lengths are all within 1% accuracy. More importantly, the ratio of $a_0(\mathrm{MEAM})/a_0(\mathrm{DFT})$ shows no more systematic decrease with increasing Z, unlike the conventional EAM potentials. Similar statements hold for the binding energies, which are shown in figure 8. Now, errors are within 6%, except for the tetrahedron and the triangular tiling, which deviate by -7.5% and +11.5%, respectively. The stiffnesses also turn out very satisfactory, i.e, mostly within $O(15\%)$

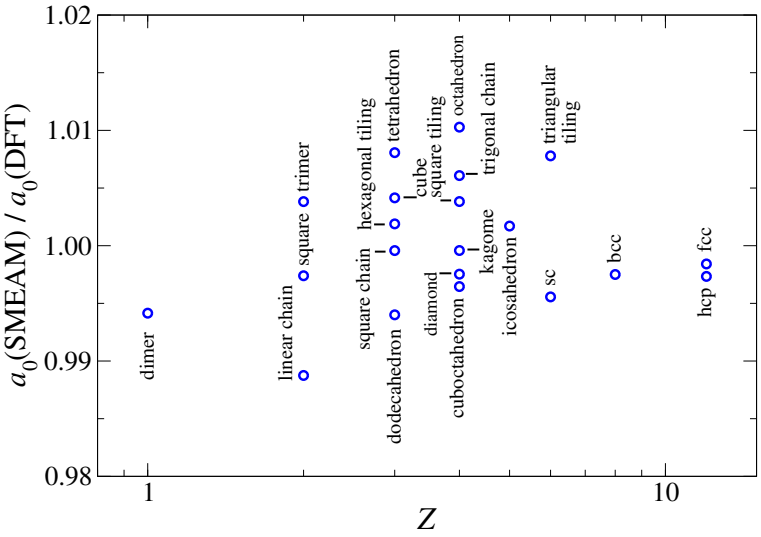

Figure 7. SMEAM equilibrium length a_0(SMEAM) divided by the DFT equilibrium length a_0(DFT) as a function of the coordination number Z for different geometries.

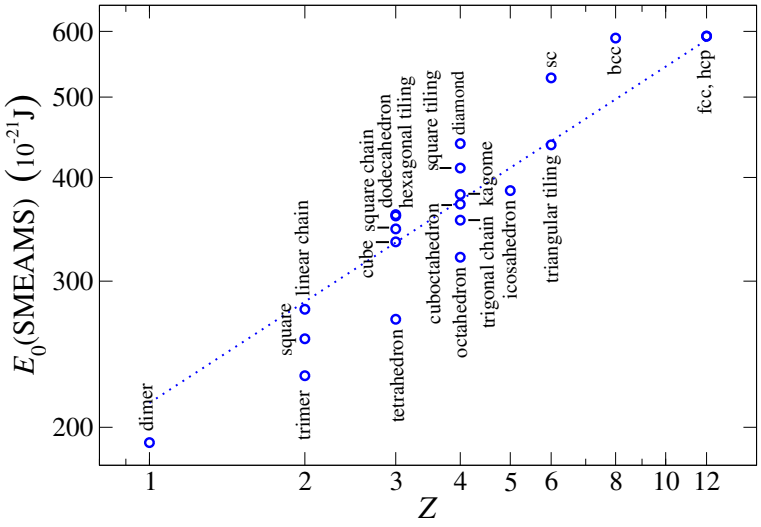

Figure 8. SMEAM results for the binding energy E_0(SMEAM) as a function of the coordination number Z for different geometries. The dotted line is identical to that drawn in figure 1.

as revealed in figure 9. Only the trimer and the diamond structure show deviations of approximately 20%. Again no systematic trends with either coordination number, dimension or openness of the structure appear to be obvious.

The beneficial effect of SMEAM corrections on binding energies and stiffnesses can be understood in a straightforwad fashion within the nearest-neighbor approximation (see section 2.3) of the modified Gupta potential. Through the modification, A is

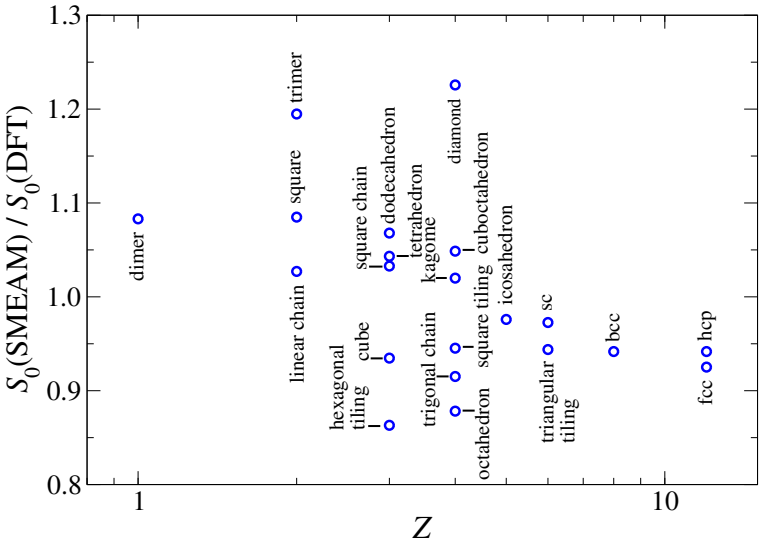

Figure 9. EAM equilibrium stiffness S(EAM) divided by the DFT stiffness S(DFT) as a function of the coordination number Z for different geometries.

effectively replaced as follows

$$A \to A\left(1 + \sum_n I_n c_n\right), \tag{39}$$

where I_n is the value for an invariant of the nearest-neighbor shell, which depends on the nature of the lattice, n enumerates the invariants, and c_n is an atom- or element-specific parameter. For the invariant $I_H = \rho_{i\alpha\alpha}$, we find $I_H(\text{n.n.}) = Z$, if only nearest-neighbors (n.n.) are included. Thus, for a fixed value of Z, this term cannot bias planar or low-dimensional over three-dimensional structures, which is why including this invariant into the potential does not improve the fits. However, the invariant $I_{\text{H2}'}(\text{n.n.}) = \rho^2_{i\alpha\beta}$ yields Z^2/D for most inversion-symmetric structures, e.g., linear chain, simple cubic crystal, etc. Even the non-inversion-symmetric diamond structure satisfies $I_{\text{H2}'}(\text{n.n.}) = Z^2/D$. Thus, depending on the prefactor $c_{\text{H2}'}$, low-dimensional structures at a given value of Z turn out energetically higher or lower than high-dimensional structures with the same coordination number.

In addition to isotropic volume changes, we also computed the response of selected structures to non-isotropic deformation. For fcc and sc, results were satisfactory, although the elastic tensor of these structures were not included into the parameter fit. Specifically, for fcc we found dimensionless Cauchy violations of $\tilde{C}^{\text{fcc}}_{\text{Cauchy}}(\text{SMEAM}) = 0.3440$ vs $\tilde{C}^{\text{fcc}}_{\text{Cauchy}}(\text{DFT}) = 0.2947$, while the isotropy violations were $\tilde{C}^{\text{fcc}}_{\text{iso}}(\text{SMEAM}) = -0.2971$ vs $\tilde{C}^{\text{fcc}}_{\text{iso}}(\text{DFT}) = -0.3809$. For simple cubic systems, the numbers were less satisfactory, i.e., $\tilde{C}^{\text{sc}}_{\text{Cauchy}}(\text{SMEAM}) = 0.1320$ vs $\tilde{C}^{\text{sc}}_{\text{Cauchy}}(\text{DFT}) = 0.6794$, while the isotropy violations turned out $\tilde{C}^{\text{sc}}_{\text{iso}}(\text{SMEAM}) = 0.5474$ vs $\tilde{C}^{\text{sc}}_{\text{iso}}(\text{DFT}) = 0.3017$. Unfortunately, the elastic tensor was not satisfactory at all for the diamond structure. Here, we found $\tilde{C}^{\text{dia}}_{\text{Cauchy}}(\text{SMEAM}) = -0.0127$ vs $\tilde{C}^{\text{dia}}_{\text{Cauchy}}(\text{DFT}) = -0.6741$, while the

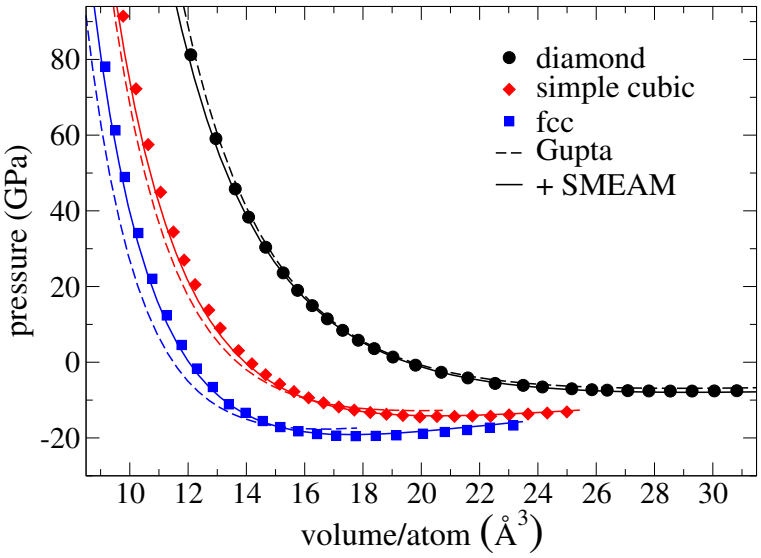

Figure 10. Pressure as a function of the volume per atom for three different crystalline structures. Symbols show DFT results, while dashed and full lines refer to reparametrised Gupta potentials with and without SMEAM corrections, respectively.

isotropy violations were $\tilde{C}_{\rm iso}^{\rm dia}({\rm SMEAM}) = -1.5875$ vs $\tilde{C}_{\rm iso}^{\rm dia}({\rm DFT}) = -0.8096$. The large discrepancies for the elastic tensors between SMEAM and DFT of diamond could not be fixed by including these properties into the fit. The same statement holds for all modified EAM potentials mentioned in this section. While MEAM potentials for four-coordinated structures have been devised successfully, [23, 72] their transferability to other structures remains to be tested. For the broad set of structures investigated here, it might necessary to include many-body effects in the repulsion, whose functional form affects elastic properties more strongly than binding energies. Nonetheless, preliminary tests using Rosen repulsion terms [73] did not prove successful.

Although the full elastic tensor is not described very accurately for either the diamond or the simple cubic structure, the equation of state is reproduced quite well for these two phases over a pressure range of more than 100 GPa in addition to that of the fcc structure, as shown in figure 10. Interestingly, the SMEAM correction to the Gupta potential improve all shown EOS in the full pressure range, i.e., for structures that are much compressed or stretched compared to those entering the fits.

Lastly, we note some results on defect energies, even if the presence of defects implies inequivalent atoms and thus the possibility of charge transfer, which, as argued in the introduction, is beyond the capability of conventional EAM potentials. For point defects, charge transfer effects should nevertheless be small: For most mono-atomic systems, one might assume that electronegativity and chemical hardness change as a function of the number of nearest neighbors and thus differences between 11 and 12-coordinated atoms should be marginal. In fact, for "vertical" point vacancies in fcc (i.e., no structural relaxation of atoms near the defect) we find that the Gupta-SMEAM potential predicts defect energies of 1.84×10^{-19} J, which is 10% less than the 2.05×10^{-19} J value from DFT.

In contrast, surface energies are overestimated. Now the Gupta-SMEAM prediction is 1.45 J/m^2 for a (111) surface, which exceeds the DFT results 1.36 J/m^2 by 6%. Further surface energies together with selected results for elastic moduli are listed in tables 2 and 3.

4. Conclusions

In this work, we found that a reparametrisation of the simple four-parameter Gupta EAM potential produced satisfactory results for a broad set of copper structures. DFT data on bond lengths were typically reproduced within 1.5%, the binding energies within $O(10\%)$, and stiffness parameters or bulk moduli within $O(20\%)$. This level of accuracy is almost on par with that of our reference DFT calculations. Changing the functional form of the Gupta potential, such as increasing the complexity of the charge density within the EAM framework, the embedding function, or the two-body repulsion, usually somewhat deteriorated the fits but never improved them beyond a few per cents. We found two possibly beneficial alterations. The first is to replace the Friedel expression for the embedding term with a parametrisation of the embedding function through the Birch-Murnahan equation of state, which, however, needs to produce the correct dissociation limit. The second alteration consists of replacing the exponential decay of the charge density with a $1/R^6$ dependence as used in the Finnis-Sinclair potential,[34] however, while keeping everything else as in Gupta. Both changes, however, reduce the χ^2 function only marginally while impeding analytical treatments. An advantage of the $1/R^6$ expression is that it is numerically cheaper than the exponential function.

One reason why adding complexity to Gupta's EAM does not help much is that conventional EAM potentials intrinsically cannot reproduce certain trends for copper. All conventional EAM potentials automatically favor structures with large coordination over those with small coordination number independent of the geometry. As a consequence, the propensity of copper to form planar or low-dimensional structures is intrinsically underestimated in EAM potentials. For example, four copper atoms are predicted to rather form a tetrahedron than a square, in contrast to DFT results. Similar statements hold for other geometries and other elements.

The Gupta EAM description can be improved by adding terms that also contain gradients or higher-order derivatives of density to either the (effective) density or the embedding function, as proposed in the context of the quasi-atom model. [20] By adding square-gradient corrections to the EAM potential alone (one single fit parameter, i.e., the prefactor to the term $\propto \rho_{i\alpha}^2$), errors already decrease by a little more than 30%. This improvement is similar to that obtained by adding square-gradient density corrections to an EAM-based description of aluminum. [48] Additional terms are needed to further correct the energetics of planar or low-dimensional structures, such as the invariant $\rho_{i\alpha\beta}^2$, whose neareast neighbor contribution for most inversion-symmetric systems turns out proportional to Z^2/D. Including this invariant together with square-gradient and the third power of the square gradient brings down the error to 50% compared to

our reparametrisation of the simple Gupta potential. The parameters for these cases are summarised in Table 1. Adding terms proportional to another invariant considered previously in MEAM, $\rho^2_{i\alpha\beta\gamma}$, or any invariant formed with less than three pairs of indices, does not improve the results by more than fractions of one percent. The latter statement also holds for the invariant $\rho_{i\alpha\alpha\beta\beta}$, even if its prefactor can be fixed to accurately accout for the fcc-hcp energy difference.

We conclude that despite, or perhaps because of, its simplicity, the Gupta potential from 1981 [28] combined with square-gradient density and higher-order corrections as proposed by Scott and Zaremba [20] clearly outperforms the later, standard (modified) embedded atom methods, [32, 38, 74] at least when considering our set of structures ranging from clusters to bulk phases. Rather than replacing the simple functional form of the Gupta-SMEAM approach with elaborate expressions, it might be beneficial to introduce entirely new features. One such addition could be to couple SMEAM to a charge transfer approach in such a way that the electronegativity and potentially the chemical hardness of an atom becomes environment dependent.

Acknowledgments We thank the Jülich Supercomputing Centre for providing us with computing time and Lars Pastewka, Wolf Dapp, and Lingti Kong for helpful discussions.

Appendix

In this appendix, we summarize our results for the interaction parameters of the Gupta potential and its modifications as well as some selected results produced by the potential.

Table 1. Force-field parameters for different levels of approximation.

	V_R (10^{-15}J)	σ_R (Å)	A (10^{-18}J)	σ_Q (Å)	c_G2	$c_{\mathrm{H2}'}$	c_G6
Gupta	1.5597	0.2284	-1.318	0.6404	N.A.	N.A.	N.A.
Gupta+SG	0.6588	0.2583	-2.251	0.5325	-0.1981	N.A.	N.A.
SMEAM	0.4660	0.2741	-3.275	0.4859	-0.3778	-0.1528	0.2812

Table 2. Selected results for the fcc structure from different levels of approximation. Elastic tensor elements are stated in units of GPa, surface energies $S(xyz)$ in J/m^2 as function of the orientation xyz, and point defect energies in units of 10^{-18} J.

	C_{11}(fcc)	C_{12}(fcc)	C_{44}(fcc)	$S(111)$	$S(110)$	$S(100)$	E(point)
Gupta	164	115	81	1.45	1.64	1.53	0.215
Gupta+SG	159	117	70	1.12	1.21	1.31	0.187
SMEAM	160	122	67	1.45	1.62	1.74	0.184
DFT	164	128	80	1.36	1.44	1.66	0.205

Table 3. Elastic constants for the simple cubic and diamond lattice in GPa.

	C_{11}(sc)	C_{12}(sc)	C_{44}(sc)	C_{11}(dia)	C_{12}(dia)	C_{44}(dia)
Gupta	275	2.7	-24	34	57	42
Gupta+SG	253	14	-22	37	57	44
SMEAM	263	15	-20	42	58	59
DFT	136	80	-13	85	36	93

[1] Foiles S M and Adams J B 1989 *Phys. Rev. B* **40** 5909–5915
[2] LeSar R, Najafabadi R and Srolovitz D J 1991 *J. Chem. Phys* **94** 5090–5097
[3] Daw M S, Foiles S M and Baskes M I 1993 *Mat. Sci. Rep.* **9** 251–310
[4] Mishin Y, Mehl M J, Papaconstantopoulos D A, Voter A F and Kress D J 2001 *Phys. Rev. B* **63** 224106–1–224106–14
[5] Dong Y, Li Q and Martini A 2013 *J. Vac. Sci. Technol. A* **31** 030801
[6] Thomas Jr J F 1971 *Scripta Metall.* **5** 787–790
[7] Davis H L and Noonan J R 1983 *Surf. Sci.* **126** 245
[8] Lindgren S A, Walldén L, Rundgren J and Westrin P 1984 *Phys. Rev. B* **29** 576
[9] Abell G C 1985 *Phys. Rev. B* **31** 6184–6196
[10] Guevara J, Weissmann M and Llois A M 1994 *J. Phys.: Condens. Matter* **6** 3939
[11] Rogal J, Divinski S V, Finnis M W, Glensk A, Neugebauer J, Perepezko J H, Schuwalow S, Sluiter M H F and Sundman B 2014 *Phys. Stat. Sol. (a)* **251** 97 – 129
[12] Schaefer H E 1987 *Phys. Stat. Sol. (a)* **102** 47 – 65
[13] Koehler J S 1941 *Phys. Rev.* **60** 397
[14] Kuhlmann-Wilsdorf D 1999 *Phil. Mag. A* **79** 955 – 1008
[15] Ercolessi F, Tosatti E and Parrinello M 1986 *Phys. Rev. Lett.* **57** 719
[16] Ercolessi F and Adams J B 1994 *Europhys. Lett.* **26** 583
[17] Finnis M W 1988 *Phil. Mag. A: Cond. Matt.* **58** 143–163
[18] Jacobsen K W, Stoltze P and Nørskov J K 1996 *Surf. Sci.* **366** 394
[19] Jacobsen K W, Nørskov J K and Puska M J 1987 *Phys. Rev. B* **35** 7423
[20] Stott M J and Zaremba E 1980 *Phys. Rev. B* **22** 1564
[21] Ludwig M, Farkas D, Pedraza D and Schmauder S 2002 *Modelling Simul. Mater. Sci. Eng.* **14** 9187–9206
[22] Mendelev M I, Kramer M J, Becker C A and Asta M 2008 *Phil. Mag.* **88** 1723–1750
[23] Lee B J, Ko W S, Kim H K and Kim E H 2010 *Calphad* **34** 510–522
[24] Jalkanen J, Rossi G, Trushin O, Granato E, Ala-Nissila T and Ying S C 2010 *Phys. Rev. B* **81** 041412(R)
[25] Streitz F H and Mintmire J W 1994 *Phys. Rev. B* **50** 11996
[26] Nistor R A, Polihronov J G, Müser M H and Mosey N J 2006 *J. Chem. Phys.* **125** 094108
[27] Engin C, Sandoval L and Urbassek H M 2008 *Modelling Simul. Mater. Sci. Eng.* **16** 035005–035016
[28] Gupta R P 1981 *Phys. Rev. B* **23** 6265–6270
[29] Norskov J K and Lang N D 1980 *Phys. Rev. B* **21** 2131–2136
[30] Ackland G J 2012 1.10 - interatomic potential development *Comprehensive Nuclear Materials* ed in Chief: Rudy JM Konings E (Oxford: Elsevier) pp 267 – 291
[31] Daw M S 1989 *Phys. Rev. B* **39** 7441
[32] Daw M S and Baskes M I 1984 *Phys. Rev. B* **29** 6443–6453
[33] Clementi E and Roetti C 1974 *At. Data Nucl. Data Tables* **14** 177–478
[34] Finnis M W and Sinclair J E 1984 *Phil. Mag. A: Cond. Matt.* **50** 45–55
[35] Sutton A P and Chen J 1990 *Phil. Mag. Lett.* **61** 139–146
[36] Norskov J K and Lang N D 1982 *Phys. Rev. B* **26** 2875–2885
[37] Baskes M I, Nelson J S and Wright A F 1989 *Phys. Rev. B* **40** 6085

[38] Baskes M I 1992 *Phys. Rev. B* **75** 2727–2742
[39] Vinet P, Rose J H, Ferrante J and Smith J R 1989 *J. Phys.: Condens. Matter* **1** 1941–1963
[40] Birch F 1947 *Phys. Rev.* **71** 809
[41] Daniels W B and Smith C S 1958 *Phys. Rev.* **111** 713–721
[42] Zinman J M (ed) 1969 *The Physics of Metals* (New York: Cambridge University Press)
[43] Friedel J and Sayers C M 1977 *J. Phys.* **38** 697
[44] Horsfield A P, Bratkovsky A M, Fearn M, Pettifor D G and Aoki M 1996 *Phys. Rev. B* **53** 12694–12712
[45] Puska M J, Nieminen R M and Manninen M 1981 *Phys. Rev. B* **24** 3037–3047
[46] Tersoff J 1988 *Phys. Rev. B* **37** 6991–7000
[47] Pagonabarragaa I and Frenkel D 2001 *J. Chem. Phys.* **115** 5015–5026
[48] Wu G, Lu G, Garcia-Cervera C J and Weinan E 2009 *Phys. Rev. B* **79** 035124
[49] Giannozzi P, Baroni S, Bonini N, Calandra M, Car R, Cavazzoni C, Ceresoli D, Chiarotti G L, Cococcioni M, Dabo I, Corso A D, Fabris S, Fratesi G, de Gironcoli S, Gebauer R, Gerstmann U, Gougoussis C, Kokalj A, Lazzeri M, Martin-Samos L, Marzari N, Mauri F, Mazzarello R, Paolini S, Pasquarello A, Paulatto L, Sbraccia C, Scandolo S, Sclauzero G, Seitsonen A P, Smogunov A, Umari P and Wentzcovitch R M 2009 *J. Phys.: Condens. Matter* **21** 395502
[50] Perdew J P, Burke K and Ernzerhof M 1996 *Phys. Rev. Lett.* **77** 3865–3868
[51] Perdew J P, Burke K and Ernzerhof M 1997 *Phys. Rev. Lett.* **78** 1396
[52] Goedecker S, Teter M and Hutter J 1996 *Phys. Rev. B* **54** 1703–1710
[53] Kresse G and Joubert D 1999 *Phys. Rev. B* **59** 1758–1775
[54] Rappe A M, Rabe K M, Kaxiras E and Joannopoulos J D 1990 *Phys. Rev. B* **41** 1227(R)–1230(R)
[55] Martyna G J and Tuckerman M E 1999 *J. Chem. Phys.* **110** 2810
[56] Overton Jr W C and Gaffney J 1955 *Phys. Rev.* **98** 969
[57] Rohlfing E A and Valentini J J 1986 *J. Chem. Phys.* **84** 6560–6566
[58] Prieto F E and Renero C 1965 *J. Chem. Phys.* **43** 1050
[59] Brewer L 1968 *Science* **161** 115
[60] Smith J C (ed) 1976 *Metal Reference Book, 5th ed.* (London: Butterworths)
[61] Kittel C 2005 *Introduction to Solid State Physics, 8th ed.* (United States: John Wiley & Sons Inc.)
[62] Pauling L 1947 *J. Am. Chem. Soc.* **69** 542–553
[63] van 't Klooster P, Trappeniers N J and Biswas S N 1979 *Physica B* **97** 65
[64] Chase Jr M W, Davies C A, Downey Jr J R, Frurip D J, McDonald R A and Syverud A N 1985 *J. Phys. Chem. Ref. Data* **14** Suppl. 1
[65] Saunders N, Miodownik A P and A T D 1988 *Calphad* **12** 351
[66] Dinsdale A T 1991 *Calphad* **15** 315
[67] Wang Y, Curtarolo S, Jiang C, Arroyave R, Wang T, Ceder G, Chen L Q and Liu Z K 2004 *Calphad* **28** 79
[68] Brewer L 1967 *Acta Metall.* **15** 553 – 556
[69] Engel N 1967 *Acta Metall.* **15** 557 – 563
[70] Hume-Rothery W 1968 *Prog. Mat. Sci.* **13** 229 – 265
[71] Drautz R and Pettifor D G 2006 *Phys. Rev. B* **74** 174117
[72] Kim E H, Shin Y H and Lee B J 2007 *Calphad* **32**
[73] Rosen P 1953 *J. Chem. Phys.* **21** 1007–1012
[74] Daw M S and Baskes M I 1983 *Phys. Rev. Lett.* **50** 1285–1288